4B.5   USING VELOCITY DATA FROM NWRT PAR AND OU-PRIME TO DETERMINE DYNAMICS AFFECTING RAPID INTENSIFICATION OF AN EF4 TORNADO

Adam J. Smith[1] * David Bodine[1], Pamela L. Heinselman[2], Phillip B. Chilson[1]

[1] *Atmospheric Radar Research Center and School of Meteorology, University of Oklahoma, Norman, OK*

[2] *NOAA/OAR National Severe Storms Laboratory, Norman, OK*

1.   INTRODUCTION

During tornado events, accurate identification of a tornado signature (TS) or tornado vortex signature (TVS) is critical for providing accurate and timely tornado warnings. The update interval of a radar can greatly impact early detection of these signatures, as some tornadoes may develop or intensify in a matter of minutes, while some radars may provide volume scans every 5 min. Within these signatures, rapid increases in peak-to-peak or gate-to gate velocity differences may indicate tornado intensification. Detailed spatial sampling is needed to maximize the potential for detecting the peak winds and maximum velocity differences within a TS. Thus, some combination of high temporal and spatial sampling appears ideal when sampling tornadic storms. But this begs the question: what temporal and spatial sampling characteristics are needed to best sample a rapidly evolving tornado?

In central Oklahoma, several radars are available to examine the effects of scanning characteristics when sampling rapidly evolving tornadoes. For example, the National Weather Radar Testbed Phased-array Radar (NWRT PAR) implements several unique signal processing and electronic scanning techniques to provide volume scans in as little as 30 s (Heinselman et al. 2008, 2011). Several kilometers away, the University of Oklahoma's Polarimetric Radar for Innovations in Meteorology and Engineering (OU-PRIME) uses a 0.5^o beamwidth to provide high-resolution polarimetric observations of severe weather (Palmer et al. 2011). Also nearby is a Terminal Doppler Weather Radar (TDWR) at Ok-

lahoma City (TOKC) which has a 0.5^o beamwidth and performs volume scans in 60 s. These radars, in conjunction with the Weather Surveillance Radar—1988 Doppler (WSR-88D) at Twin Lakes, OK (KTLX), implement a variety of scanning strategies to track and analyze weather phenomena. As such, the differences in spatial and temporal resolution may be used to evaluate the effects of spatial and temporal sampling when observing intense tornadoes and other severe weather.

On 10 May 2010, an EF4 tornado developed within 10 km of TOKC, then moved to the northeast and produced EF4 damage within 10 km of KTLX. This tornado was sampled by all four radars in central Oklahoma, with customized scans implemented by both OU-PRIME (Palmer et al. 2011) and NWRT PAR (Smith et al. 2011). Throughout its lifetime, this tornado remained within 40 km of all four radars, so all radars obtained scans beneath 500 m AGL within the circulation. In this study, we use peak-to-peak velocity differences to track the rapid movement and intensification of the TS. The radar-observed tracks are compared with the observed damage path to determine whether radar trends reflect actual tornado intensity. We also examine trends in maximum reflectivity (Z_{max}) within the tornado debris signature to determine whether radar reflectivity provides evidence of significant damage. These results will help determine whether rapid updates and/or increased spatial sampling may be used to better identify locations of severe damage during a tornado event. Favorable results may also help guide the design of future radar systems.

Corresponding author address: Adam J. Smith, Atmospheric Radar Research Center and School of Meteorology, 120 David Boren Dr., Suite 4636, Norman, OK 73072-7307; *e-mail: adam.j.smith-1@ou.edu.*

2. OKLAHOMA RADARS AND SAMPLING CHARACTERISTICS

The four radars in the study include two research radars (NWRT PAR and OU-PRIME) plus two operational radars (KTLX and TOKC). Scanning characteristics for these radars are provided in Table 1. Each of the operational radars sampled continuously using a 360° volume coverage pattern, while the research radars were operated using a manually selected 90° sector. OU-PRIME provided updates in 140–160 s, while NWRT PAR sampled a series of three 4-elevation scans in 8 s, followed by a 22-elevation scan completed in 30 s. After 2240 UTC, only the full 22-elevation VCP was sampled, and the update interval increased to 60 s. Both the WSR-88D and NWRT PAR used half-beamwidth oversampling to improve azimuthal spacing. TDWR scans using a 0.5^o beamwidth, but due to system limitations, the environment is only scanned with 1.0^o beam spacing. (Weber 2000).

When dealing with different radar systems, several sampling issues need to be considered. Since TOKC and OU-PRIME operate at a frequency of 5 GHz, some signal attenuation is possible in regions of heavy precipitation. On 10 May 2010, OU-PRIME reflectivity values within the tornado debris signature are an average of 5 dBZ weaker than the other radars. Also, for NWRT PAR, no data are available within 10 km of the radar. Thus, PAR analysis begins at 2226:03 UTC, while the other radars provide continuous data starting around 2218 UTC.

3. COMPARISONS OF TORNADO PATHS FROM MULTIPLE RADARS

To examine the effects of sampling when estimating tornado location, we first examine the radar-observed circulation from each radar. Using the lowest available elevation scan, we visually locate the TS, which is defined by a region of extreme Doppler velocities with maximum values separated by several azimuths (Brown 1999). Using the center of this TS, we compile a track of TS locations as a function of time. Tracks from KTLX, TOKC and NWRT PAR are obtained using the 0.5^o elevation. OU-PRIME data

was not available for the EF4 tornado at 0.5^o, so the 1.0^o elevation is used for this study. The tracks for KTLX and OU-PRIME are displayed in Fig. 1, while TDWR and NWRT PAR results are shown in Fig. 2. An observed National Weather Service damage path is displayed for comparison, while population density is shown to demonstrate the potential impact the tornado could produce for the public.

Throughout the tornado period (2225–2248 UTC), KTLX and OU-PRIME sample a nearly linear east-northeastward track with several southward and northward deviations within the observed damage path (Fig. 1). However, the center generally remains along the northwest edge of the damage path. Despite more frequent updates from OU-PRIME, there appears to be little distinction between the two tracks. When considering more rapid updates from NWRT PAR and TOKC, the tracks more clearly exhibit several deviations within the nearly linear damage track. Again, the circulation generally remains at the northern edge of the damage path, except near the end of the event. The tracks from TOKC and NWRT PAR are nearly identical, except for some slight differences due to sampling differences to the northeast. Thus, it appears that when tracking the circulation center, rapid temporal updates do not provide significantly new information for this tornado. However, increased temporal sampling does provide increased confidence that the track is accurate and reasonable.

The initial TS develops more than a kilometer north of the initial damage path at 2225 UTC. A weak tornado briefly touched down at this time and produced damage to fences and power poles along the initial part of the circulation track (not shown). Further south along the main damage path, an intense TS is not observed, despite tornado damage and several reports of a confirmed tornado in the area. (National Weather Service Norman WFO cited 2011). However, OU-PRIME and KTLX data show a strong rear flank downdraft gust front just to the southeast of the TS (not shown). A previous analysis of this OU-PRIME data proposed that several weak circulations may have developed along the gust front and produced the initial tornado (Bodine et al. 2010). Additional studies of the TDWR and OU-PRIME data are ongoing to find additional signs of weak circula-

tions near the beginnings of the damage path.

After the intense TS approaches the damage path, all four radars show that the circulation center persists along the northwestern edge of the wide damage path. During this event, the storm moved rapidly to the northeast at speeds up to 20 m s^{-1}. Within the tornado, localized southwesterly winds were likely enhanced by the storm's propagation, while northeasterly tornado winds were reduced. Examination of NWRT PAR data showed outbound velocities (southwesterlies) exceeding 85 m s^{-1} after 2230 UTC, while inbound velocities (northeasterlies) generally did not exceed 30 m s^{-1} (not shown). Thus, the location of the circulation center may not correspond to the center of a damage region. Instead, peak radar velocities likely provide a better means of determining locations where damage is expected during a tornado event.

4. EVOLUTION OF CIRCULATION INTENSITY AND IMPACTS ON POPULATION

As shown in Section 3, the center of a large TS may not correspond to the region of greatest damage. However, trends in velocity or reflectivity could provide evidence of tornado intensification, thus indicating that significant damage is likely. Here, the evolution of peak-to-peak velocity difference (ΔV) and maximum reflectivity (Z_{max}) are examined within the tornado circulation to determine whether the highest values correspond closely to the most intense damage. The range, beam height and resolution volume are also examined to determine how temporal and spatial scanning characteristics impact the radars' capability to sample peak wind velocities. Finally, we study the population density affected by the tornado to determine whether the greatest damage occurred in more populated areas. Knowing regions of dense population can help identify locations to focus specialized warnings before the tornado hits and provide immediate assistance once the tornado moves away.

Initially, the mesocyclone and TS develop just after 2215 UTC, and all radars show a gradual increase in ΔV between 2217–2223 UTC (Fig. 3a). Z_{max} decreases slightly for all radars (Fig. 3b), but

does not show a significant debris signature yet. Shortly thereafter, ΔV increases rapidly from 60 m s^{-1} to 120 m s^{-1} between 2225 and 2231 UTC. Maximum reflectivity also increases from 40 dBZ to 58 dBZ during this period, indicating rapid tornado intensification and larger debris are likely being sampled. The intensification is first visible using NWRT PAR and TOKC data over a one-minute period (2228–2229 UTC), while the increase is not fully visible using OU-PRIME or KTLX until 2231 UTC. The increases in ΔV and Z_{max} correspond closely with an observed increase in damage intensity, indicating the tornado intensified rapidly in a span of roughly one minute. Therefore, while all radars detect the rapidly intensifying tornado, more rapid updates from NWRT PAR and TOKC provide detection of the intensification nearly three minutes before KTLX and OU-PRIME. After 2232 UTC, the maximum reflectivity remains relatively steady for all radars, and does not appear to show any trends that indicate increased damage at the ground.

After peaking at 2233 UTC, ΔV begins to decrease for all radars except KTLX, which samples the largest ΔV at 2240 UTC. This time corresponds with the period of greatest damage, but only KTLX detects the most intense circulation. However, upon examining the tornado's range from each radar (Fig. 4a), the storm is approximately 8 km from KTLX, while the other radars are more than 25 km away. These ranges correspond to a beam height of 80 m for KTLX and 300 m for all other radars (Fig. 4b). An examination of resolution volume size (Fig. 5) shows that since the tornado is closest to KTLX, its resolution volume are smaller, thus providing better resolution of the circulation. This resolution may also allow for better observations of peak winds within the tornado.

Finally, to examine the connection between tornado damage and the amount of structures impacted, we examine the population density affected by the tornado during its lifetime (Fig. 6). A map of the population density is also displayed in Figs. 1–2. The tornado initially developed in a higher density region of business along Interstate 35, then moved into a region of scattered farms and homes to the northeast (2225–2230 UTC). Despite the higher population, damage was limited to fences, trees and roofs

as the tornado was initially weak. As it continued to the east, the tornado moved over a small lake (2231–2232 UTC) and rapidly intensified. Shortly thereafter, the tornado demolished several homes (2233–2235 UTC) over several rural blocks. The most significant EF4 damage was observed around 2236–2237 UTC as a number of newly built homes were knocked down in a subdivision near Interstate 40. Several more homes and two gas station were destroyed near I-40 around 2240 UTC, then the tornado moved into a rural area, damaging several outbuildings before weakening (2242–2251 UTC). Based on this damage survey, we do find that the greatest EF4 damage was observed in a region with moderate population density. However, early in the event, the tornado developed and produced less severe damage in a more densely populated region near Interstate 35. Therefore, the population density appear can provide an indicator of the potential threat a tornado may cause. However, detailed radar observations are still needed to assess the true intensity of damage as the tornado impacts an area.

5. CONCLUSIONS

In this study, we examine the evolution of an intense tornado signature as sampled by four Oklahoma radars on 10 May 2010. The center of the observed tornado signature is tracked using each radar, and trends in the peak-to-peak velocity difference and maximum reflectivity are tracked to analyze tornado development and intensification. All radars showed very similar circulation tracks, but frequent ($<$60 s) updates from TOKC and NWRT PAR provided additional confidence that the circulation center generally remained to the northern edge of the damage path. Sudden increases in peak-to-peak velocity difference (ΔV) and maximum velocity (Z_{max}) also show that the tornado signature intensified rapidly around 2228 UTC, and TOKC and NWRT PAR showed evidence of intensification 3 min prior to KTLX and OU-PRIME. During the most intense damage, KTLX sampled the strongest circulation when the tornado was only 8 km away. The more distant radars were unable to sample the peak winds at that range due to larger resolution volumes sampling the mesocyclone instead of the tornado. In

these cases, a range correction technique may be useful to improve wind speed estimates (e.g., Newman et al. 2011). However, greater spatial and temporal sampling may also provide improved tracking of tornado characteristics in real time.

While the maximum reflectivity from TOKC and NWRT PAR showed signs of tornado intensification around 2228 UTC, it is difficult to find specific trends that denote regions of potential damage. However, polarimetric data from OU-PRIME have shown several tornado debris signatures that are not detected within reflectivity (Bodine et al. 2010). Further analysis of both reflectivity and polarimetric fields may uncover further signs of tornado damage during and after intensification. Additional studies are also needed to better determine the effects of spatial sampling when observing tornadoes with different radar systems. The close proximity of TDWR, NWRT PAR and OU-PRIME may facilitate additional comparison studies, including those that occur at greater ranges from the radar. A comparison of the NWRT PAR with the co-located KOUN WSR-88D or mobile radars may also provide a more objective comparison of temporal and spatial sampling without the need to consider a target's range. Finally, additional analysis of population density may provide new insight into the relationships between population density and observed damage. Determining the correlation between circulation intensity and the severity of damage may provide new insight into the costs and impacts that intense tornadoes may leave on society.

6. ACKNOWLEDGEMENTS

References

Bodine, D., R. D. Palmer, C. Ziegler, and P. L. Heinselman, 2010: High-resolution radar analysis during tornadogenesis from OU-PRIME on 10 May 2010. Extended abstracts, *25th Conference on Severe Local Storms*, Denver, CO, Amer. Meteor. Soc., 15.4.

Brown, R. A., 1999: Nomogram for aiding the interpretation of tornadic vortex signatures measured by Doppler radar. *Wea. Forecasting*, **13**, 505–512.

Heinselman, P., S. Torres, D. LaDue, and H. Lazrus, 2011: 2010 phased-array radar innovative sensing experiment. Extended abstracts, *27th Conference on Interactive Information Processing Systems (IIPS)*, Seattle, WA, Amer. Meteor. Soc., 12B.4.

Heinselman, P. L., D. L. Priegnitz, K. L. Manross, T. M. Smith, and R. W. Adams, 2008: Rapid sampling of severe storms by the National Weather Radar Testbed Phased Array Radar. *Wea. Forecasting*, **23**, 808–824.

National Weather Service Norman WFO, cited 2011: Storm data and unusual weather phenomena—May 2010. [Available online at: `http://www.srh.noaa.gov/media/oun/stormdata/oun201005.pdf`.]

Newman, J. F., V. Lakshmanan, P. L. Heinselman, and T. M. Smith, 2011: Range correction for radar-derived azimuthal shear: Applications to a tornado detection algorithm. Extended abstracts, *27th Conference on Interactive Information Processing Systems (IIPS)*, Seattle, WA, Amer. Meteor. Soc., 8B.4.

Palmer, R. D., and Coauthors, 2011: Observations of the 10 May 2010 tornado outbreak using OU-PRIME. *Bull. Amer. Meteor. Soc.*, **92**, 871–891.

Smith, A. J., P. B. Chilson, and P. L. Heinselman, 2011: Using the NWRT PAR to evaluate temporal sampling during two rapidly evolving tornado events. Extended abstracts, *27th Conference on Interactive Information Processing Systems (IIPS)*, Seattle, WA, Amer. Meteor. Soc., 13B.4.

Weber, M. E., 2000: FAA surveillance radar data as a complement to the WSR-88D network. Extended abstracts, *9th Conference on Aviation, Range and Aerospace Meteorology*, Orlando, FL, Amer. Meteor. Soc., J1.10.

Table 1: Scanning characteristics for the four Oklahoma radars analyzed in this study.

Radar	Frequency	True Beamwidth	Azimuthal Spacing	Gate Width	Update interval
KTLX	3.0 Ghz (S-band)	1.0^o	0.5^o	250 m	240 s
OU-PRIME	5.5 GHz (C-band)	0.5^o	0.5^o	125 m	180 s
TOKC	5 GHz (C-band)	0.5^o	1.0^o	150 m	60 s
NWRT PAR	3 GHz (S-band)	$1.5–2.1^o$	$0.75–1.0^o$	240 m	8–60 s
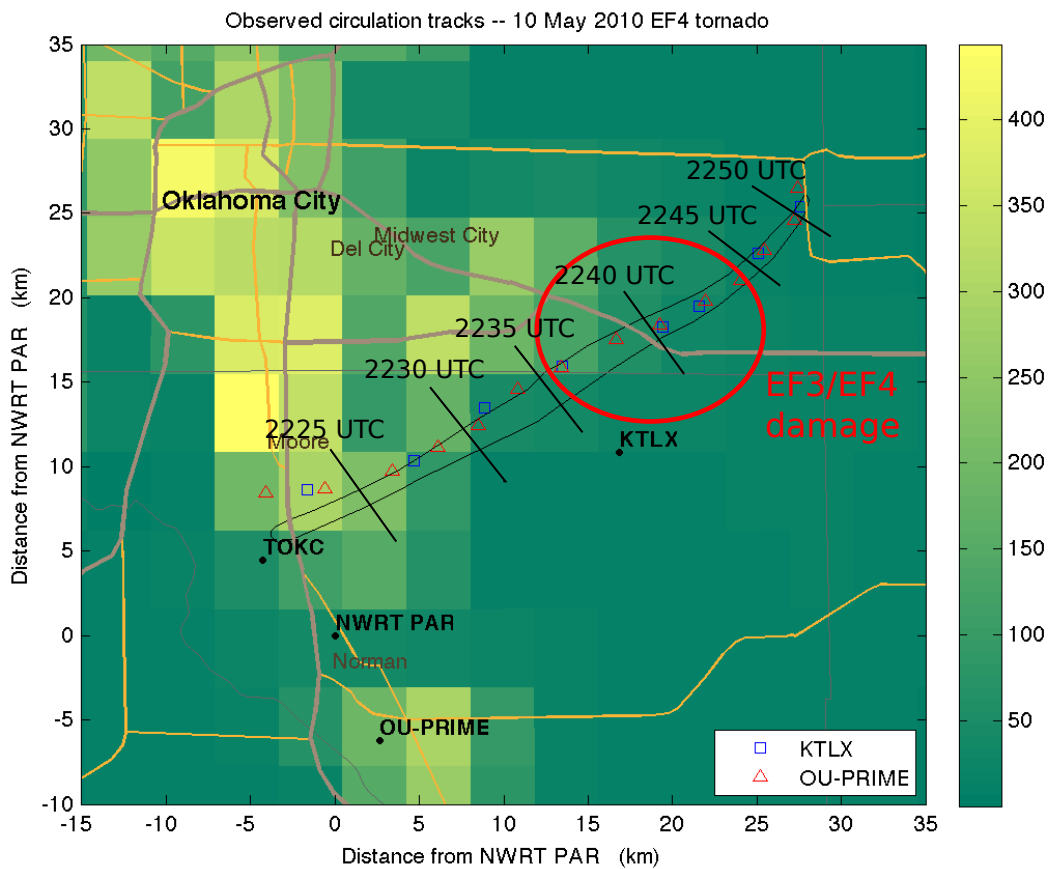
Figure 1. A map showing the locations of radar-observed circulation centers, the observed damage path on 10 May 2010. A red circle indicates the region of EF3 and EF4 damage within the damage path. Radars shown include KTLX (4-min updates) and OU-PRIME (3 min updates). The background image shows the 2010 population density in central Oklahoma.
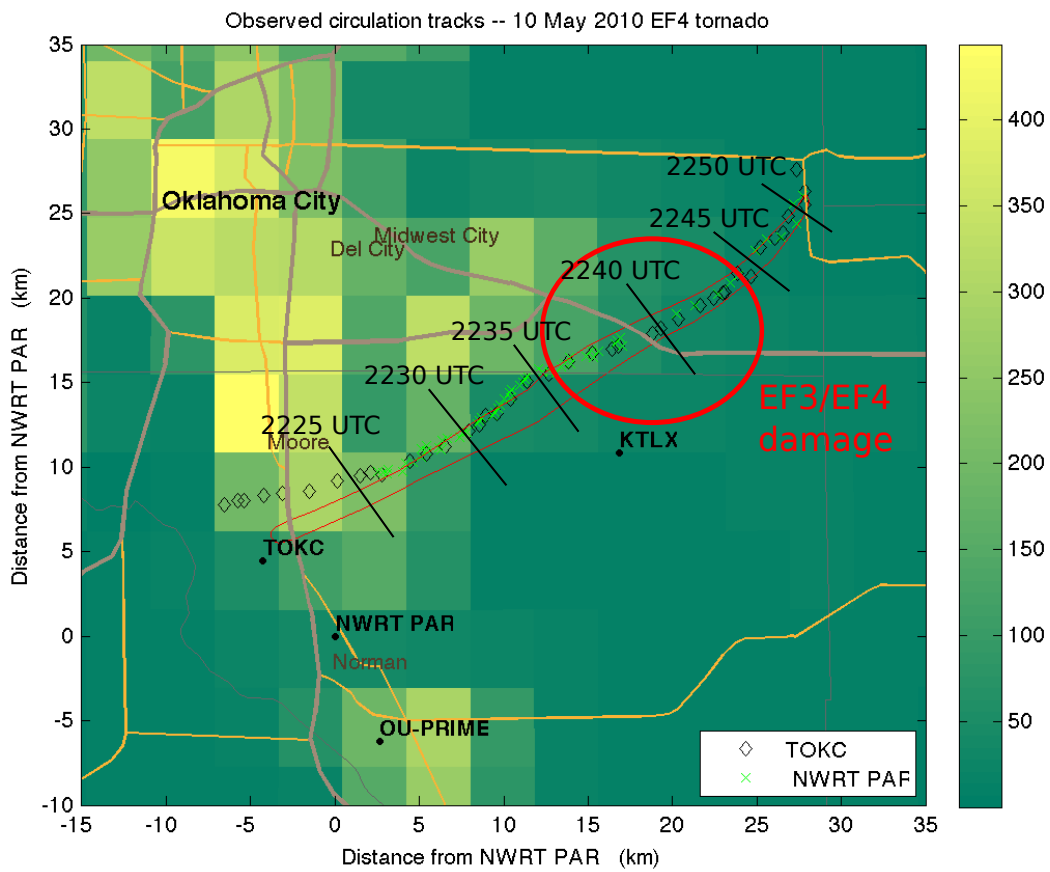
Figure 2. Same as Fig. 1, except showing circulation centers as sampled by TOKC (30–60 s updates) and NWRT PAR (8–60 s updates). The NWRT PAR data begins at 2226 UTC due to sampling issues within 10 km of the radar.
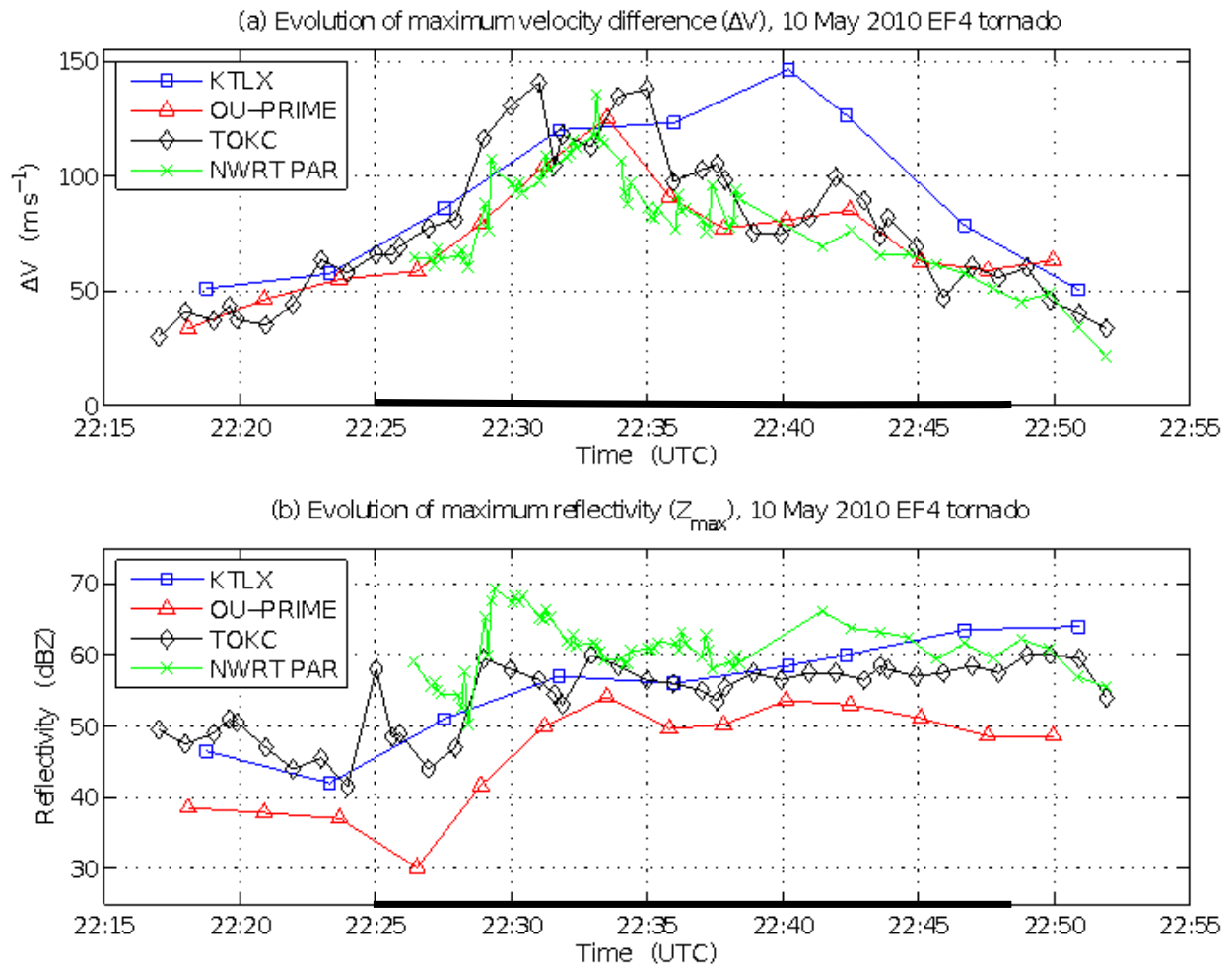
Figure 3. (a) Time evolutions of the peak-to-peak velocity difference (ΔV) within the observed TS. A solid black line indicates the period when the tornado was on the ground. Note that NWRT PAR data are only available starting at 22:26 UTC. All radars use an elevation angle of 0.5^o except OU-PRIME which uses an elevation of 1.0^o. (b) Maximum reflectivity observed within the tornado debris signature.
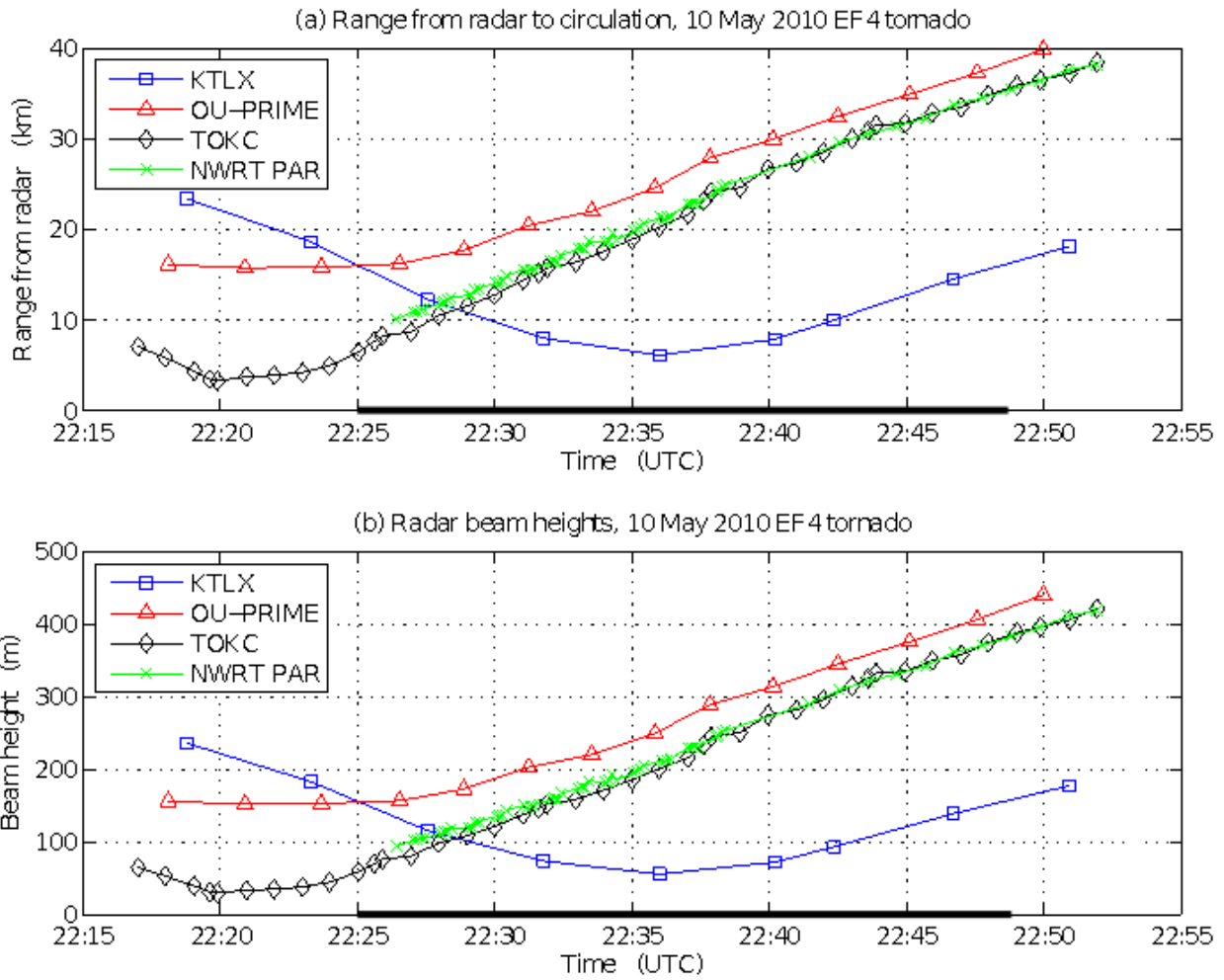
Figure 4. (a) Ranges from each radar to the observed circulation as observed by each radar. A solid black line denotes the period when the tornado was on the ground. (b) Same as (a), except showing beam heights calculated based on the circulation's range and the radar elevation angle.
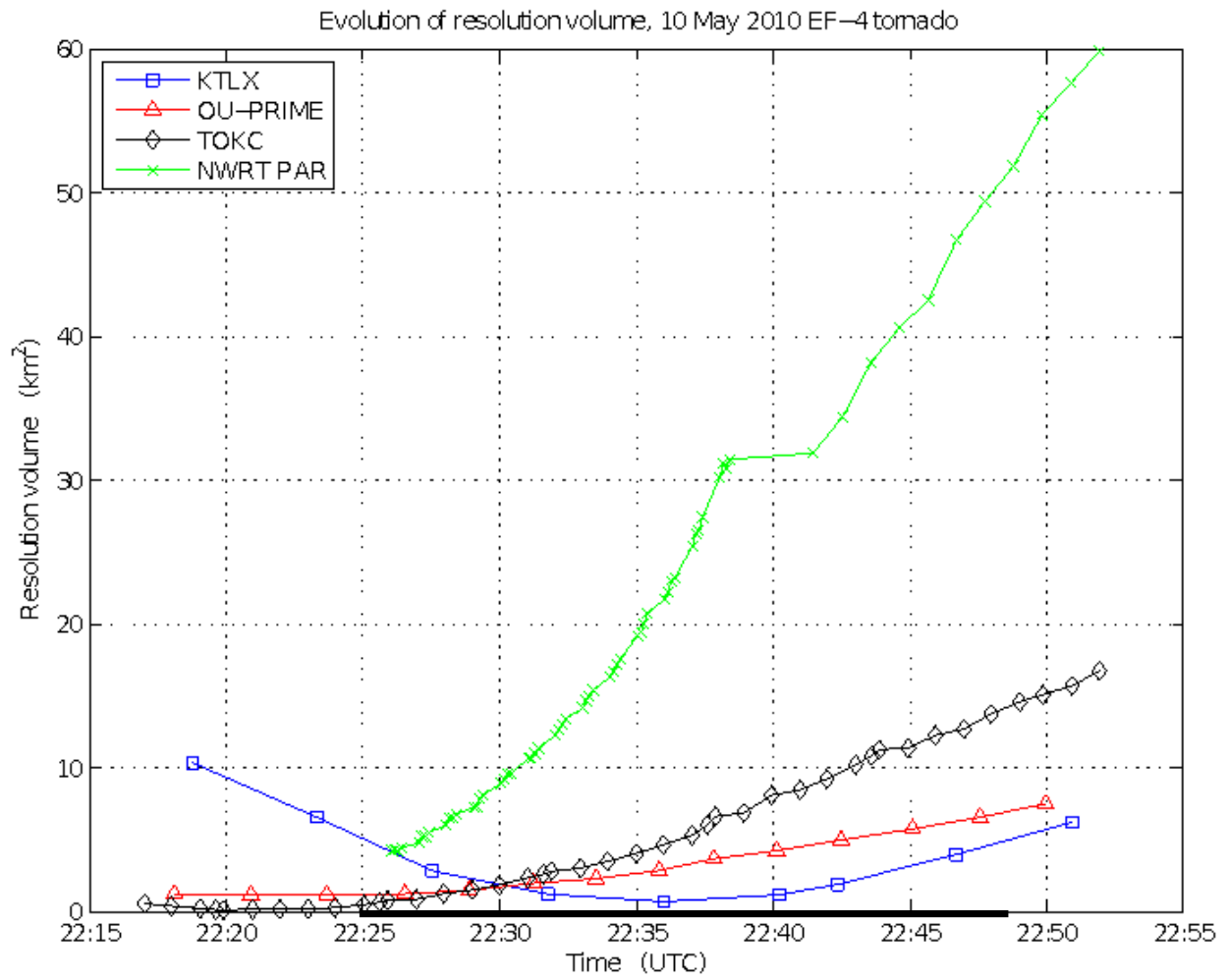
Figure 5. Changes in resolution volume size for each radar as the circulation moves to the northeast.
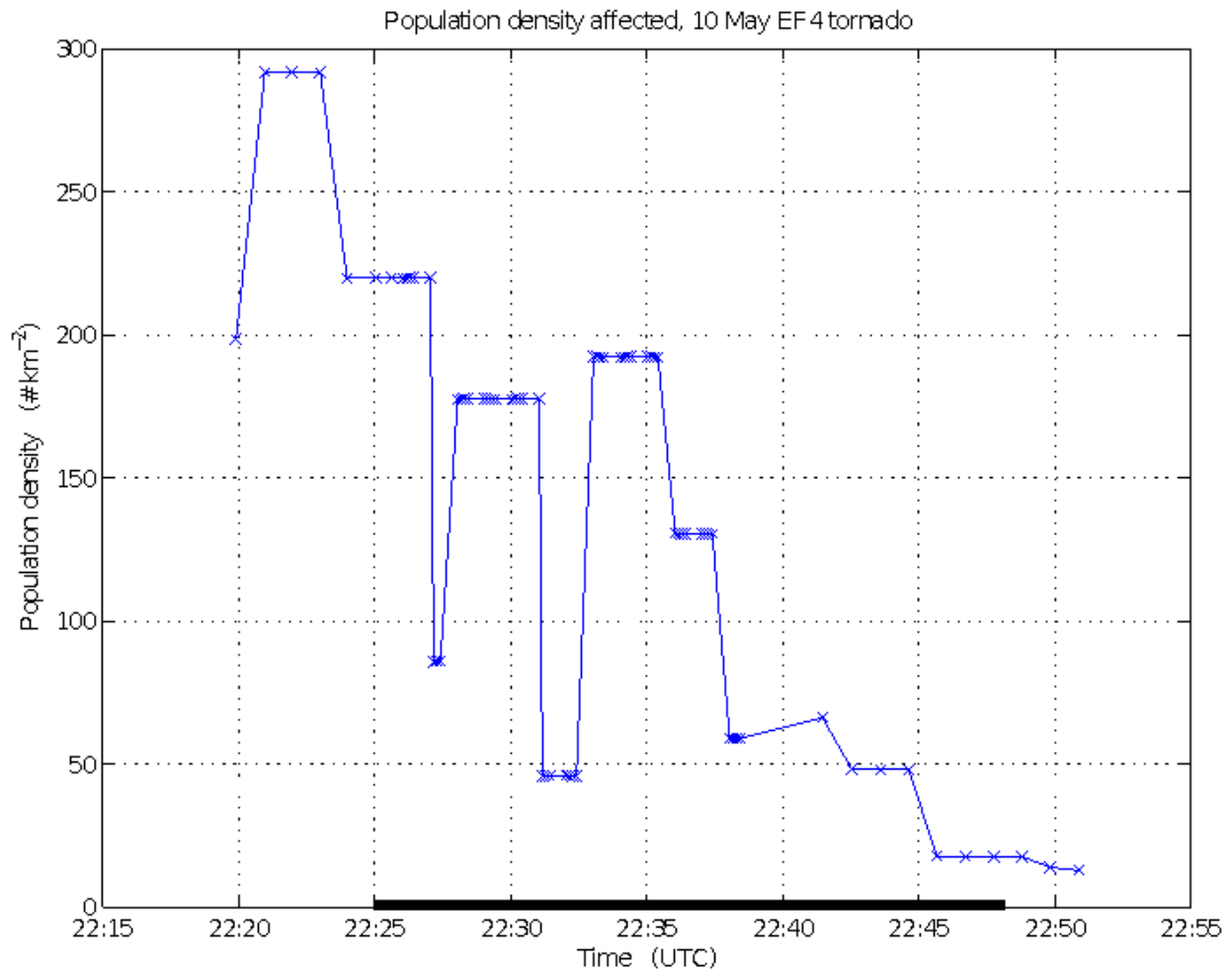
Figure 6. A time series showing the population density affected by the EF4 tornado over time. Values from 22:20–22:25 correspond to 1-min TOKC updates, while 22:26–22:38 were obtained using 8–30 s updates from NWRT PAR. After 22:38, only 1-min updates are available using NWRT PAR. (See Figs. 1–2 for a comparison of circulation tracks and the affected population density.